Frequency stabilization of a fiber laser to rubidium: a high-accuracy 1.53 μm wavelength standard

Sarah L. Gilbert

Electromagnetic Technology Division
National Institute of Standards and Technology, 325 Broadway, Boulder, CO 80303

ABSTRACT

Spectroscopy of the rubidium $5P_{3/2} \rightarrow 4D_{5/2}$ transition near 1.529 μm has been performed using a single-longitudinal-mode erbium-doped fiber laser. Rubidium atoms were laser-cooled and confined in a vapor-cell Zeeman optical trap. This produced a dense sample of cold atoms and reduced the Doppler broadening of the transition to less than the natural linewidth. Transition linewidths of 10 MHz were observed on the $5P_{3/2} \rightarrow 4D_{5/2}$ transition and the fiber laser was actively stabilized to the $5P_{3/2}$, $F=3 \rightarrow 4D_{5/2}$, $F'=3$ line of ^{87}Rb.

1. INTRODUCTION

A goal of the NIST wavelength standard research is to produce primary wavelength standards, in the optical communications regions, which are stable and reproducible to better than 1 MHz. Accurate wavelength standards are important for many of the proposed optical communication schemes involving wavelength division multiplexing, frequency division multiplexing, and coherent detection. At present, the 1.5 μm region is favored for optical communication due to the success of the erbium-doped fiber amplifier. I have developed a wavelength standard scheme which uses a 1.5 μm fiber laser stabilized to narrow resonances in laser-cooled rubidium. Other research on wavelength standards in the 1.5 μm region has concentrated on the stabilization of diode lasers to various atomic (krypton,[1] neon,[2] and rubidium[3,4,5]) and molecular (ammonia,[6,7] water,[6] and acetylene[8,9]) lines. Unfortunately, the frequency noise spectrum of diode lasers can extend well beyond 1 GHz. A fiber laser's frequency fluctuations, on the other hand, are dominated by mechanical motion of the cavity elements and thermal drift.[10] The spectrum of the fluctuations is therefore confined to low frequencies (<1 kHz) where they can be easily removed by an electronic servo loop.

Atomic and molecular reference lines in the 1.5 μm region are not ideal; atomic transitions are between excited states or involve frequency doubling of the probe light. Molecular lines are weak overtone or combination bands. Atomic rubidium has several strong absorption lines which can serve as wavelength references for optical communications. Figure 1 is an energy level diagram showing the these transitions. The $5P_{3/2} \rightarrow 4D_{3/2}$ and the $5P_{3/2} \rightarrow 4D_{5/2}$ transitions near 1.529 μm provide several lines. A two-step excitation scheme is required: the $5S_{1/2} \rightarrow 5P_{3/2}$ transition at 780 nm followed by the $5P_{3/2} \rightarrow 4D$ transitions. Another set of references can be obtained by frequency-doubling 1.560 μm light and probing the 780 nm $5S_{1/2} \rightarrow 5P_{3/2}$ transition. A set of references near 1.324 μm can be observed in another two-step excitation scheme: the $5S_{1/2} \rightarrow 5P_{1/2}$ transition at 795 nm followed by the $5P_{1/2} \rightarrow 6S_{1/2}$ transition. All of these lines can be probed in both ^{85}Rb and ^{87}Rb isotopes contained in the same cell.

0-8194-1038-1/93/$4.00

In earlier work,[11] I performed two-step excitation of rubidium by sending 780 nm diode laser light and a counterpropagating beam of 1.529 μm light from a fiber laser through a room temperature cell of ^{87}Rb. In the counterpropagating geometry, the 1.529 μm transition linewidth was nearly Doppler-free since only a narrow velocity distribution of atoms was excited by the diode laser. I observed a linewidth of 14 MHz (FWHM) on the 1.529 μm transitions and stabilized the fiber laser and diode laser to their respective transitions. Sasada[4] and Tetu[5,12] have also used two-step excitation of Rb and have stabilized 1.3 μm and 1.5 μm diode lasers to both the $5P_{1/2} \rightarrow 6S_{1/2}$ and $5P_{3/2} \rightarrow 4D$ transitions. Sasada observed linewidths of 10-15 MHz on the 1.5 μm transitions. Unfortunately, the large linewidths of the diode lasers caused transition linewidths greater than 50 MHz for the 1.3 μm transitions and for the 1.5 μm transitions in Ref. 5. Sasada has measured the frequencies of these 1.3 μm and 1.5 μm lines to an accuracy of about 40 MHz.

To improve on my previous work and produce a highly stable primary wavelength standard, I have constructed a vapor-cell Zeeman optical trap (ZOT) for neutral rubidium. The Doppler broadening of optical transitions is negligible in a ZOT trap since the atoms are laser-cooled to below 1 mK.[13] Pressure shifts arising from collisions with background gas are also significantly reduced due to the low pressure maintained by an ion pump. Combining this with the low frequency noise of the fiber laser yields a stable, reproducible standard with a high signal-to-noise ratio.

2. EXPERIMENTAL DETAILS

2.1 Fiber laser

I have constructed a single-longitudinal-mode erbium-doped fiber laser and have used it for spectroscopy of acetylene[10] and rubidium.[11] A schematic diagram of the Er^{3+} fiber laser is shown in Fig. 2, and the laser characteristics are discussed in more detail in Ref. 10. The standing-wave laser is in a V-shaped folded-cavity configuration. In one arm of the cavity, two short pieces of Er-doped fiber are pumped through a mirror (high reflectance at 1.53 μm) by 528.7 nm light from an Ar^+ laser. A 1200 groove/mm diffraction grating, used in Littrow configuration, is positioned at the end of the other cavity arm. The output is coupled through the folding mirror, which has a transmittance of about 20% at 1.53 μm. The fibers form coupled cavities within the longer cavity; the overlap of the transmission peaks of these cavities selects a single longitudinal mode. Coarse tuning of the wavelength from 1.52 μm to 1.58 μm is accomplished by manually tilting the diffraction grating. The laser can be finely tuned, without mode hops, over 2 GHz by translating the grating with a piezo-electric transducer (PZT) and stretching one of the fibers with another PZT. The output power of the fiber laser is about 3 mW at 1.53 μm.

I evaluated the fiber laser's frequency noise[10] and determined that the short-term frequency fluctuations ($f \geq 5$ Hz) of the free-running laser were less than 1 MHz rms. A spectrum analysis of this noise from 0 to 25 kHz showed no structure beyond 600 Hz. The high frequency contribution (frequencies >2 kHz) to the linewidth of an erbium-doped ring fiber laser was measured to be less than 1.4 kHz[14] using a delayed self-heterodyne technique.

2.2 Vapor-cell Zeeman optical trap

The apparatus for the ZOT vapor-cell optical trap is similar to those described in Refs. 13 and 15. A schematic diagram of the trap is shown in Fig. 3. Three orthogonal pairs of counterpropagating laser beams with opposite helicity intersect in a cell containing about 10^{-6} Pa ($\approx 10^{-8}$ Torr) of natural abundance rubidium. A spatially varying dc magnetic field in the intersection region causes position-dependent shifts of the Zeeman levels of the Rb atoms. When the laser is tuned to the low frequency side of the 780 nm $5S_{1/2} \rightarrow 5P_{3/2}$ transition, the atoms experience a position-dependent radiation pressure. The atoms in the low-velocity tail of the room temperature Maxwell-Boltzmann distribution are slowed by the radiation pressure and trapped in the intersection region.

The vapor cell is a 12 cm long glass tube with a 2 cm x 2 cm square cross section and a window on one end. The other end is connected to a stainless steel vacuum system with a window to provide laser beam access. A 2-l/s ion pump maintains a background pressure at less than 10^{-6} Pa. Rubidium vapor is allowed to enter the system through a valve until the Rb vapor pressure reaches about 10^{-6} Pa. The magnetic field gradient is produced by two coils with counterpropagating currents. The coils are in an anti-Helmholtz configuration, where the distance between the coils is equal to their 2.7 cm radius. The field is zero at the center of the trap and the gradient is ~ 0.15 T/m (15 G/cm).

Figure 4 shows the energy levels of ^{87}Rb which are pertinent to this experiment. The trapping laser beams come from a 780 nm diode laser with external feedback from a diffraction grating.[16] The feedback narrows the diode laser's linewidth to about 1 MHz and allows tuning of the laser frequency by tilting the grating. The trapping laser frequency is locked to the low frequency side of the $5S_{1/2}$, F=2 $\rightarrow$ $5P_{3/2}$, F=3 cycling transition by electronic feedback to a PZT controlling the grating tilt using a signal from a saturated absorption spectrometer. The laser's output is expanded to about 1 cm in diameter and divided into three 2 mW beams. The circularly polarized beams are sent through the cell along three orthogonal axes and are retroreflected back into the cell after passing through quarter-wave plates. A second diode laser (~ 1mW power) overlaps the trapping beams and is tuned to the $5S_{1/2}$, F=1 $\rightarrow$ $5P_{3/2}$, F=2 transition. This "hyperfine pump" laser optically pumps atoms out of the F=1 ground state and puts them back into the cycling transition.

I observe the 780 nm fluorescent light from the trap with a charged-coupled device video camera and also by imaging the cloud onto a silicon photodiode. The Rb fluorescence is predominantly due to the decay of the $5P_{3/2}$, F=3 level which is repeatedly excited by the trapping laser. Using the method described in Ref. 15, I estimated the number of trapped atoms by calculating the power-broadened scattering rate and light collection and detection efficiency. I estimate that about 10^7 trapped atoms are confined in a 1 mm^3 volume.

Due to the resonant nature of the trapping force, the ZOT trap is very isotope-selective. I have also trapped ^{85}Rb in this cell by tuning the diode lasers to the appropriate transitions. The trapping laser was tuned to the $5S_{1/2}$, F=3 $\rightarrow$ $5P_{3/2}$, F=4 ^{85}Rb cycling transition, and the hyperfine pump laser was tuned to the $5S_{1/2}$, F=2 $\rightarrow$ $5P_{3/2}$, F=3 ^{85}Rb transition. Due to the greater abundance of ^{85}Rb, the number of trapped atoms was larger than the number obtained for the ^{87}Rb trap. However, the hyperfine splitting of ^{87}Rb is considerably greater than that of ^{85}Rb, so I have chosen to use ^{87}Rb for the spectroscopy of the 1.529 μm $5P_{3/2} \rightarrow 4D_{5/2}$ transitions.

3. RESULTS

The hyperfine structure of the $5S_{1/2}$, $5P_{3/2}$, and $4D_{5/2}$ levels of ^{87}Rb is shown in Fig. 4. When the fiber laser is tuned into resonance with a $5P_{3/2} \rightarrow 4D_{5/2}$ transition, it removes population from the $5P_{3/2}$, F=3 level and causes a reduction in the 780 nm fluorescent light emitted by the trapped atoms. Figure 5 shows the trap fluorescence as the fiber laser is scanned through the $5P_{3/2}$, F=3 $\rightarrow$ $4D_{5/2}$, F'=4, 3, and 2 transitions under the conditions of weak trapping and hyperfine pump laser power. The effect of the fiber laser is much larger on the F=3 $\rightarrow$ F'=3 and F=3 $\rightarrow$ F'=2 "depopulation" transitions since these transitions allow the atoms to leave the $5S_{1/2} \rightarrow 5P_{3/2}$ cycling transition. The atoms must then be pumped back into the cycling transition by the hyperfine pump laser. The $5P_{3/2}$, F=3 $\rightarrow$ $4D_{5/2}$, F'=4 transition, however, is a cycling transition, resulting in a strongly coupled three-level system.

At full trapping laser power, the line shapes of the $5P_{3/2} \rightarrow 4D_{5/2}$ transitions are significantly distorted due to Stark splitting. A trace of the trap fluorescence as the fiber laser is scanned through the transitions when the trapping laser is at maximum power is shown in Fig. 6. The trapping laser was detuned by about 1.5Γ on the low frequency side of the $5S_{1/2}$, F=2 $\rightarrow$ $5P_{3/2}$, F=3 cycling transition, where Γ is the 6 MHz natural linewidth of the transition.[17] Figure 7 shows the first derivative of this signal, obtained by applying a small modulation (<100 kHz p-p) at 500 Hz on the fiber laser frequency and using phase-sensitive detection. The transitions show the Stark splitting of the energy levels due to the trapping laser power and detuning. A scan derivative where the trapping laser power was reduced to 25% of the maximum power is shown in Fig. 8. The F=3 $\rightarrow$ F'=3 and F=3 $\rightarrow$ F'=2 depopulation transitions are now nearly symmetric and have linewidths of about 10 MHz. This linewidth is predominantly due to power broadening and the 6 MHz natural linewidth of the $5P_{3/2}$ level; the natural linewidth of the $4D_{5/2}$ level is 2 MHz. The F=3 $\rightarrow$ F'=4 lineshape, however, is very distorted. This complicated dependence on fiber laser frequency is not surprising, since the fluorescence arises from the intermediate state of a strongly coupled three-level system.

The derivative signals shown in Fig. 8 for the depopulation transitions are good error signals for stabilization of the fiber laser. I sent this error signal to the fiber laser grating PZT and actively stabilized the fiber laser to the $5P_{3/2}$, F=3 $\rightarrow$ $4D_{5/2}$, F'=3 transition. The lock point for stabilization is indicated in Fig. 8. When the fiber laser was stabilized, the fluctuations of the error signal with a 10 ms time constant corresponded to fiber laser frequency excursions of less than 400 kHz p-p. The unstabilized fiber laser fluctuations within this bandwidth were about 1 MHz p-p.

4. CONCLUSIONS

I have performed high resolution spectroscopy of the 1.529 μm $5P_{3/2} \rightarrow 4D_{5/2}$ transition of laser-cooled ^{87}Rb confined in a vapor-cell Zeeman optical trap. Observing changes in the 780 nm trap fluorescence while scanning a fiber laser through the $5P_{3/2} \rightarrow 4D_{5/2}$ transition is a sensitive technique for detection of this transition. I have measured transition linewidths of 10 MHz and have stabilized the fiber laser to the $5P_{3/2}$, F=3 $\rightarrow$ $4D_{5/2}$, F'=3 transition. The good signal-to-noise ratio and narrow linewidths observed demonstrate the potential of this technique. It should be possible to obtain linewidths near the 2 MHz natural linewidth of the $5P_{3/2} \rightarrow 4D_{5/2}$ transition and a wavelength standard reproducibility of 100 kHz.

Many steps must be finished before the primary wavelength standard research is complete. The lineshapes observed on the $5P_{3/2} \rightarrow 4D_{5/2}$ transitions need to be studied in more detail, both experimentally and theoretically. Possible systematic errors, such as light shifts, magnetic fields, and variations in the detuning of the trapping laser, that could cause frequency shifts of the lock point must be studied and measured. To evaluate the absolute stability of the standard, two independent setups will be compared and their relative stability measured. The same trap apparatus can be used to produce standards based on the 780 nm (probed with frequency doubled 1.56 μm light) and 1.32 μm lines in both ^{85}Rb and ^{87}Rb.

I also plan to make several improvements to the apparatus. As pointed out in Ref. 15, the trapping efficiency of the vapor-cell ZOT improves as the diameter of the trapping beams is increased. This is due to the fact that atoms with higher velocities can be captured because of the increased slowing distance. I plan to increase the size of the trapping beams while maintaining the same laser power, thereby improving the trap and reducing the light shift due to the trapping laser intensity. I also plan to improve the fiber laser by using Bragg reflection gratings within the fiber core[18] in place of the input mirror and the diffraction grating. This would improve the free-running stability of the laser and would substantially reduce the losses in the cavity, enabling diode laser pumping. We have built an apparatus for making fiber gratings using cw uv light and have produced gratings with up to 80% reflectivity at 1.53 μm. In addition, it would be interesting to investigate the narrow-linewidth capability of fiber lasers by stabilizing them to high finesse cavities using a higher bandwidth servo system.

5. ACKNOWLEDGMENTS

I gratefully acknowledge the support of the Naval Command, Control and Ocean Surveillance Center and thank C. Wieman for useful discussions and D. Wineland and C. Weimer helpful suggestions on the manuscript.

6. REFERENCES

1. Y.C. Chung and C.B. Roxlo, "Frequency-locking of a 1.5 μm DFB laser to an atomic krypton line using optogalvanic effect," *Electron. Lett.*, Vol. 24, pp. 1048-1049, 1988.

2. S.G. Menocal, N. Andreadakis, J.S. Patel, J. Werner, C.E. Zah, T.P. Lee, and P.F. Liao, "Frequency locking of 1.5 μm DFB laser diode to a neon lamp using the optogalvanic effect," *IEEE Photon. Technol. Lett.*, Vol. 1, pp. 285-287, 1989.

3. M. Ohtsu and E. Ikegami, "Frequency stabilisation of 1.5 μm DFB laser using internal second harmonic generation and atomic ^{87}Rb line," *Electron. Lett.*, Vol. 25, pp. 22-23, 1989.

4. H. Sasada, "Wavenumber measurements of sub-Doppler spectral lines of Rb at 1.3 μm and 1.5 μm," *IEEE Photon. Technol. Lett.*, Vol. 4, 1992.

5. M. Breton, N. Cyr, P. Tremblay, and M. Tetu, "Use of rubidium vapor to frequency lock a 1.5-μm DFB laser," this conference, paper 1837-19.

6. M. Ohtsu, H. Kotani, and H. Tagawa, "Spectral measurements of NH_3 and H_2O for pollutant gas monitoring by 1.5 μm InGaAsP/InP lasers," *Japan. J. Appl. Phys.*, Vol. 22, pp. 1553-1557, 1983.

7. T. Yanagawa, S. Saito, and Y. Yamamoto, "Frequency stabilization of 1.5-μm InGaAsP distributed feedback laser to NH_3 absorption lines," *Appl. Phys. Lett.*, Vol. 45, pp. 826-828, 1984.

8. S. Sudo, Y. Sakai, H. Yasaka, and T. Ikegami, "Frequency-stabilized DFB laser module using 1.53159 μm absorption line of C_2H_2, *IEEE Photon. Technol. Lett.*, Vol. 1, pp. 281-283, 1989.

9. F. Bertinetto, "Frequency stabilization of DFB laser diodes to the P(3) line of acetylene at 1.52688 μm by external phase modulation," this conference, paper 1837-21.

10. S.L. Gilbert, "Frequency stabilization of a tunable erbium-doped fiber laser," *Opt. Lett.*, Vol. 16, pp. 150-152, 1991.

11. S. L. Gilbert, "High Resolution Spectroscopy Using Fiber Lasers," Tenth International Conference on Laser Spectroscopy, TENICOLS '91, edited by M. Ducloy, E. Giacobino, and G. Camy, pp. 359-364, World Scientific, Singapore, 1992.

12. R. Boucher, M. Breton, N. Cyr, and M. Tetu, "Dither-free absolute frequency locking on a 1.3 μm DFB laser on ^{87}Rb," *IEEE Photon. Technol. Lett.*, Vol. 4, pp. 327-329, 1992.

13. C. Monroe, W. Swann, H. Robinson, and C. Wieman, "Very Cold Trapped Atoms in a Vapor Cell," *Phys. Rev. Lett.*, Vol. 65, pp.1571-1574, 1990.

14. K. Iwatsuki, H. Okamura, and M. Saruwatari, "Wavelength-tunable single-frequency and single polarisation Er-doped fibre ring-laser with 1.4 kHz linewidth," *Electron. Lett.*, Vol. 26, pp. 2033-2035, 1990.

15. K. Lindquist, M. Stephens, and C. Wieman, "Experimental and theoretical study of the vapor-cell Zeeman optical trap," *Phys. Rev. A*, Vol. 46, pp. 4082-4090, 1992.

16. C.E. Wieman and L. Hollberg, "Using diode lasers for atomic physics," *Rev. Sci. Instrum.*, Vol. 62, pp. 1-20, 1991.

17. O.S. Heavens, "Radiative Transition Probabilities of the Excited States of the Alkali Metals," *J. Opt. Soc. Am.*, Vol. 51, pp. 1058-1061, 1961.

18. G. Meltz, W.W. Morey, and W.H. Glenn, "Formation of Bragg gratings in optical fibers by a transverse holographic method," *Opt. Lett.*, Vol. 14, pp. 823-825, 1989.

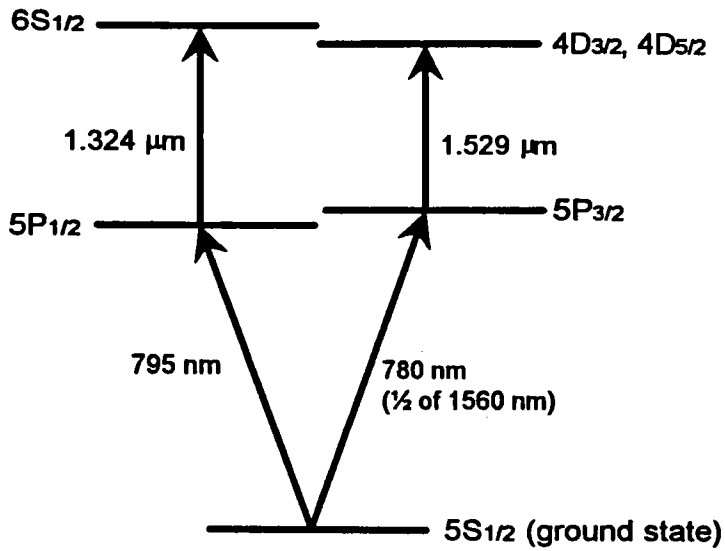

Fig. 1. Energy level diagram of rubidium showing the transitions which can be used as references for optical communication wavelength standards.

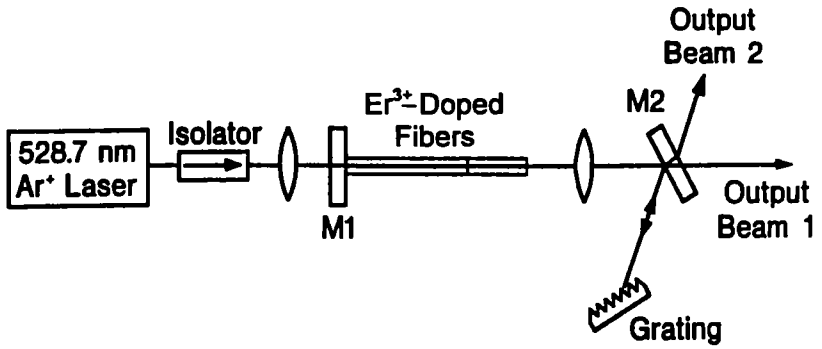

Fig. 2. Schematic diagram of the single-longitudinal-mode fiber laser. The mirror M1 (99% R at 1.53 μm, 56% T at 528.7 nm) is butted against one end of a 2.8 cm long, erbium-doped fiber. A 1 cm piece of erbium-doped fiber is attached to the longer piece.

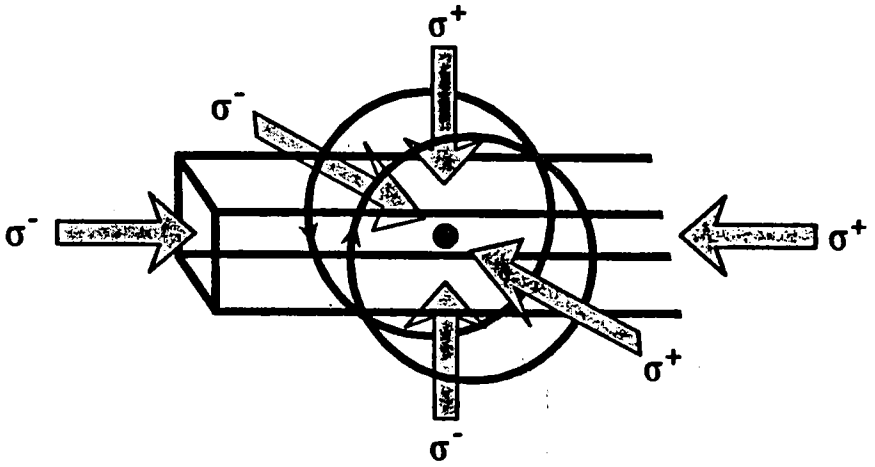

Fig. 3. Diagram of the vapor-cell ZOT trap, showing the six trapping laser beams and the magnetic field coils.

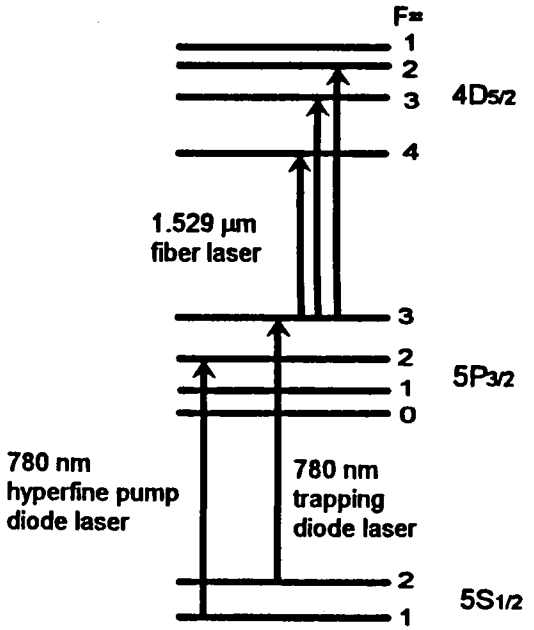

Fig. 4. Energy level diagram of ^{87}Rb showing the transitions probed in this experiment.

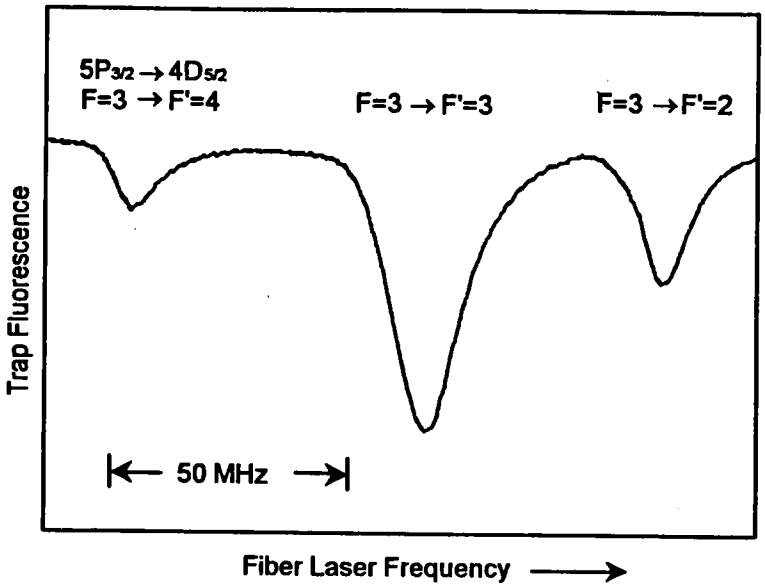

Fig. 5. Trap fluorescence (780 nm) as the fiber laser is scanned through the transitions indicated in Fig. 4 under the conditions of low trapping and hyperfine pump laser power. The reduction of trap fluorescence is 70% on the peak of the F=3 →F'=3 line.

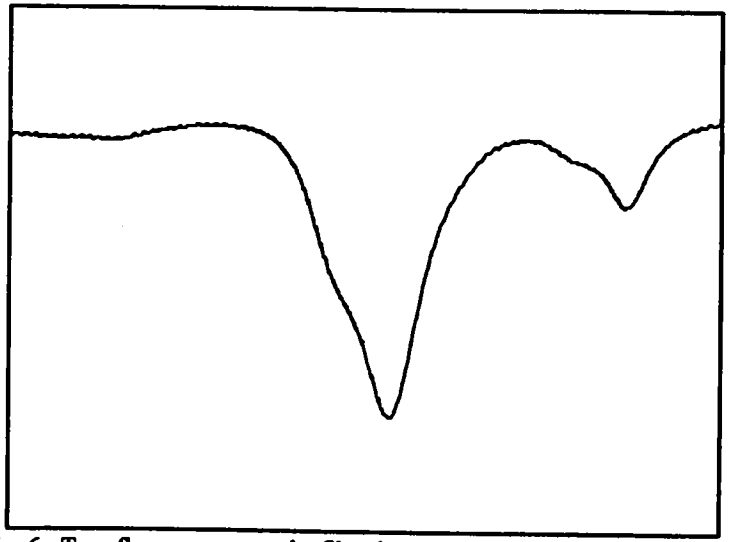

Fig. 6. Trap fluorescence as the fiber laser is scanned through the transitions when the trapping laser is at maximum power. The reduction of trap fluorescence is 30% on the peak of the F=3 →F'=3 line.

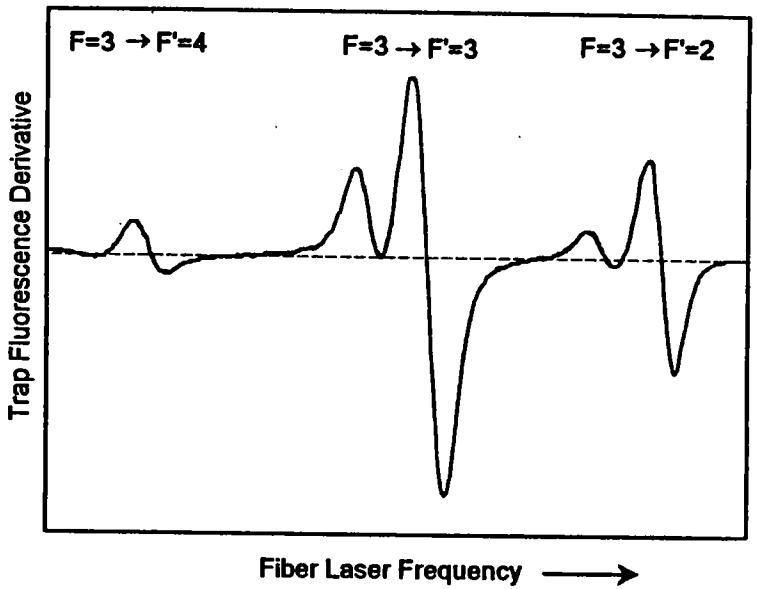

Fig. 7. First derivative of the trap fluorescence with the trapping laser at maximum power.

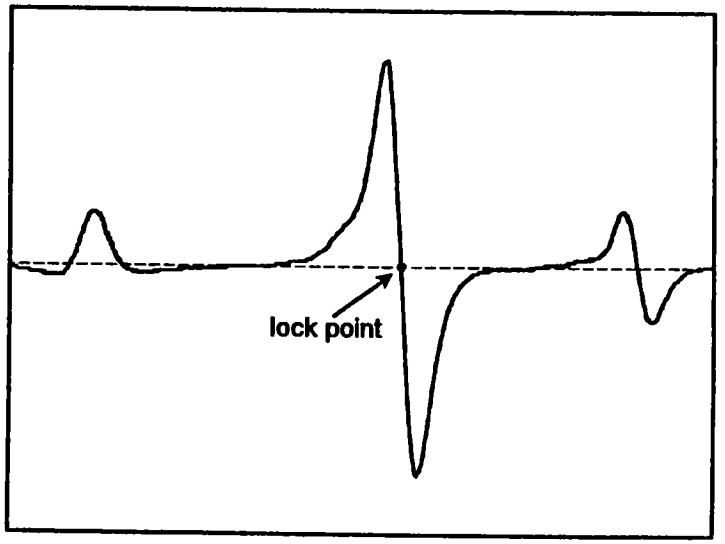

Fig. 8. First derivative of the trap fluorescence with the trapping laser at 25% of its maximum power.